BIOCHEMISTRY
including biophysical chemistry & molecular biology

Article

pubs.acs.org/biochemistry

Structural Insight into Maternal Embryonic Leucine Zipper Kinase (MELK) Conformation and Inhibition toward Structure-Based Drug Design

Giulia Canevari,* Stefania Re Depaolini, Ulisse Cucchi, Jay A. Bertrand,† Elena Casale, Claudia Perrera, Barbara Forte, Patrizia Carpinelli, and Eduard R. Felder

Nerviano Medical Sciences, Viale Pasteur 10, 20014 Nerviano, Milan, Italy

Supporting Information

ABSTRACT: Maternal embryonic leucine zipper kinase (MELK) is upregulated in several types of tumor, including breast, prostate, and brain tumors. Its expression is generally associated with cell survival, cell proliferation, and resistance to apoptosis. Therefore, the potential of MELK inhibitors as therapeutic agents is recently attracting considerable interest. Here we report the first structures of MELK in complex with AMP−PNP and with nanomolar inhibitors. Our studies shed light on the role of the MELK UBA domain, provide a characterization of the kinase active site, and identify key residues for achieving high potency, laying the groundwork for structure-based drug design efforts.

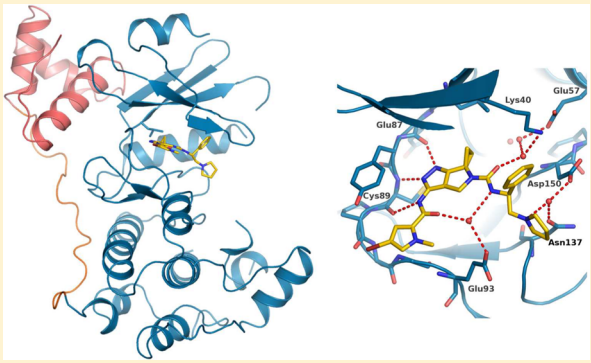

Maternal embryonic leucine zipper kinase (MELK)[1] is a member of the snf1/AMPK family of serine−threonine kinases that has been implicated in various cellular processes, including stem cell renewal, cell cycle progression, and pre-mRNA splicing. MELK is overexpressed in various undifferentiated tumors and its knockdown decreases cell-cycle progression, proliferation, and tumor growth.[2,3] MELK overexpression is reported in both breast cancer specimens and cancer cell lines, and its kinase activity possibly plays a significant role in breast cancer cell growth. In addition, a new biological role was reported for MELK in breast carcinogenesis: the kinase phosphorylates Bcl-GL, inhibiting the latter's pro-apoptotic function.[4] Moreover, Speers and co-workers described higher MELK expression in ER-negative breast cancers with respect to ER-positive breast cancers, and proposed MELK as a possible druggable target for the treatment of this breast cancer subtype.[5] MELK expression has further been found to be enriched in embryonic and adult neural stem/progenitor cells and to be required for their self-renewal capacity.[6] Increased MELK expression correlates with the pathologic grade of brain tumors, and its expression levels are significantly correlated with poor prognosis of glioblastoma, breast, and prostate cancer patients.[7−9] Recently, Chung and co-workers reported a small molecule able to inhibit MELK and to suppress the growth of breast tumor-initiating cells, indicating MELK inhibition as a potential new approach to selectively target this cell population in different tumor types.[10]

AMPK-related kinases share a similar domain organization, which comprises an N-terminal kinase domain flanked by a ubiquitin associated (UBA) domain and a C-terminal spacer sequence with, in some cases, a kinase associated domain (KA1, Figure S1, Supporting Information); in MELK the spacer is a TP-rich domain and the KA1 domain is present. The AMPK-related kinase family is the only kinase family containing UBA domains,[11] which, despite low sequence homology, generally display a typical compact three-helices bundle fold. The role of the UBA domain has not to date been fully clarified, but Beullens and co-workers have demonstrated that a construct comprising the kinase domain of MELK and the UBA domain (residues 1−340) is catalytically active, while the isolated kinase domain (residues 1−266) fails to retain activity.[12]

In search of MELK kinase inhibitors, we performed a high-throughput screening (HTS) of our proprietary compound collection, which includes kinase targeted libraries.[13] This HTS campaign led to identification of several compounds displaying good activity on MELK and prompted crystallographic studies aimed at fully characterizing the MELK active site in view of a structure-based drug design approach.

The three crystal structures reported here of unphosphorylated MELK in complex with AMP-PNP and two promising HTS hits, the benzodipyrazole Cpd1 and the pyrrolopyrazole Cpd2, are, to our knowledge, the first reported MELK structures. As such, they provide detailed structural insight into protein−inhibitor interactions and offer an opportunity for structure-assisted optimization of these HTS hits and the further development of MELK inhibitors.

Received: May 9, 2013
Revised: July 15, 2013
Published: August 5, 2013

   dx.doi.org/10.1021/bi4005864 | *Biochemistry* 2013, 52, 6380−6387

MATERIALS AND METHODS

Plasmid Construction and Baculovirus Production. The human MELK catalytic domain (CD, aminoacids 2−340, encompassing the kinase and the UBA domains; BC014039) was amplified by PCR and cloned into the pDON221 with the Gateway system (Invitrogen) adding a Rhinovirus 3C cleavage site at the N-terminus and a polyhistidine tag at the C-terminus. MELK CD cDNA was then transferred into a baculovirus expression vector using the Gateway system to obtain the final vector pVL_GST-MELK CD-His6, in order to produce a protein possessing an N-terminal GST tag in addition to the C-terminal His6 tag.

In order to prepare recombinant baculovirus, the pVL_GST-MELK CD-His6 was coinfected in Sf9 cells with BaculoBright (BD), and the virus was amplified for three cycles.

Expression and Purification of Recombinant MELK. All purification steps were performed at 4 °C. Sf21 insect cells (Invitrogen) were infected with the virus for 3 days at 27 °C, and the cellular pellet was lysed by homogenization with a Gaulin homogenizer (Niro Soavi). The lysate was applied to a Ni-Sepharose column (GE Healthcare), and after extensive washes the bound protein was eluted with imidazole. After addition of 20 mM DTT and 0.5 mM EDTA, eluted protein was loaded onto a GSH-sepharose resin and incubated for 2 h. After extensive washing, PreScission protease was added overnight in order to cleave the N-terminal GST tag.

The resulting purified enzyme (Figure S2A, Supporting Information) was analyzed by LC/MS, which revealed a content of 35% monophosphorylated and 65% unphosphorylated protein (Figure S2B, Supporting Information). This preparation was used for assay development and HTS.

To produce a more homogeneous protein for structural studies, a dephosphorylation step was performed by incubation with Lambda phosphatase; the treated protein was subsequently subjected to gel filtration using a Sephadex 200 column (GE Healthcare) equilibrated with 50 mM Tris pH 7.6, 500 mM NaCl, 5% glycerol and 1 mM DTT. The resulting protein was completely monomeric (Figure S3, Supporting Information), and the final yield was approximately 10 mg per billion cells. The purified enzyme was analyzed by LC/MS, which confirmed complete dephosphorylation of the protein (Figure S4B, Supporting Information). This pure and homogeneous enzyme (Figure S4A, Supporting Information) was used for crystallographic experiments.

Mass Spectrometry Analysis. LC−MS analyses were performed by reverse-phase chromatography on a capillary HPLC system (HP Agilent 1100 HPLC) coupled to a single quadrupole mass spectrometer HP 1100MSD (Agilent Technologies). A Poroshell 300SB-C3, 5 μm, 2.1 mm i.d., 7.5 cm (Agilent Technologies) was operated at a flow rate of 0.2 mL/min running a 20 min gradient, starting with 5% buffer B (0.05% trifluoroacetic acid in acetonitrile) in buffer A (0.05% trifluoroacetic acid in water), ending with 100% buffer B. The samples analyzed were 12 μg of purified proteins.

The mass spectrometer was operated in the positive ion mode using an electrospray ion source. Mass spectra were recorded between m/z 600 and m/z 2000. The mass spectrometer and the spectrum deconvolution were controlled and conducted using the A.09.03 LC/MSD Chem Station software suite (Agilent).

High Throughput Screening (HTS) Assay. Kinetic parameters were evaluated in matrix-design studies varying ATP and substrate concentrations, at different reaction times (see Figure S5A, Supporting Information).

HTS was performed in a KinaseGlo format using 0.75 nM MELK, 1 μM ATP, and 150 μM peptidic substrate. Upon reconfirmation in the same assay format, the IC_{50} of positive compounds were calculated in radioactive Dowex assay format adapted in 384-well plates.[14]

Kinase Assays. Automated kinase assays were conducted as described by Pevarello and co-workers.[14] The biochemical activity of compounds was determined by incubation with specific enzymes and substrates, followed by quantitation of the phosphorylated product. Compounds were 4-fold serially diluted from 10 to 0.0006 mM and then incubated for 60 min at room temperature in the presence of ATP/$P^{33}\gamma$-ATP mix [= $2K_m$], substrate [$\geq 3K_m$], and specific enzyme in a final volume of 15 μL of kinase buffer, in 384-well plates. The reaction buffer for each kinase in the panel is optimized in order to obtain a maximal signal/background ratio in a final dimethyl sulfoxide (DMSO) concentration of 1%. 60 μL of Dowex resin (Supelco) in formate pH 3.00 buffer, was added to capture unreacted $P^{33}\gamma$-ATP, thereby stopping the reaction and effecting separation from phosphorylated substrate, which remained in solution. After 60 min of rest, 22 μL of the resulting supernatant was transferred to Optiplate 384 well plates. After addition of 50 μL of Microscint 40 (Packard), radioactivity was counted using a TopCount instrument (Packard).

Cell Culture and Reagents. The human tumor cell lines A2780, LnCaP, and MDA-MB-468 were obtained from the ATCC (Rockville, MD, USA) and cultured in RPMI 1640 medium containing 10% fetal bovine serum (FBS), 2 mmol/L L-glutamine (Gibco, Grand Island, NY, USA), 100 U/mL penicillin, and 100 mg/mL streptomycin (Gibco). Cells were maintained at 37 °C in a humidified atmosphere containing 5% CO_2. Test compounds were dissolved in DMSO at a concentration of 10 mM, stored at −20 °C and diluted in cell culture medium immediately before use.

Cells Proliferation Assay. Cells were seeded in 96-well plates at final densities ranging from 10 000 to 30 000 cells per cm^2 in medium containing 10% FCS. After 24 h cells were treated with serial dilutions of compound in 2 replicates. Seventy-two hours after the treatment, cell growth was evaluated using the Cell TiterGlo assay (Promega). IC_{50} values were calculated using a sigmoidal fitting using the Assay Explorer software suite (MDL). At least two independent determinations were performed for each compound.

Western Blot Analysis. Cells were lysed in SDS buffer (125 mM Tris pH 6.8 and 2% SDS). Protein concentration was determined using a BCA Protein assay (Pierce). Proteins were resolved by SDS-PAGE and transferred to Protran nitrocellulose filters (Whatman). Antibodies against p53, GAPDH, and PARP were obtained from from Santa Cruz Biotechnology. Antibody against MELK was from Cell Signaling.

Crystallization. Rectangular prism-shaped crystals of dephosphorylated MELK (2−340) grew in hanging drops incubated at 20 °C after mixing 1 μL of protein solution at a concentration of 5−8 mg/mL with 1 μL of reservoir solution containing 6−10% PEG 3350, 200 mM NaCl, and 100 mM Bis Tris pH 6.5. Early streak seeding or microseeding was essential in order to obtain diffraction quality crystals, sized approximately 150 × 50 × 50 μm.

Data Collection and Structure Solution. Crystals were immersed in a cryoprotectant solution (10% PEG 3350, 200

dx.doi.org/10.1021/bi4005864 | Biochemistry 2013, 52, 6380−6387

mM NaCl and 100 mM Bis Tris pH 6.5 and 25% glycerol) prior to flash-cooling in liquid nitrogen. X-ray diffraction data were collected at the European Synchrotron Radiation Facility in Grenoble (ESRF beamline ID23-1) from crystals of MELK in complex with AMP-PNP, Cpd1, and Cpd2 at resolutions of 2.6 Å, 2.2 Å, and 1.85 Å, respectively. Crystals were of space group $P2_12_12_1$ (unit cell a = 60, b = 64, c = 93). Data were processed with MOSFLM,[15] merged with SCALA,[16,17] and phased via molecular replacement with Phaser,[18] using the published structure of MARK2 (PDB ID 1ZMU, 41% sequence identity) as a search model. Three distinct models were created, for the N- and C-lobes of the kinase domain and the UBA domain, in order to take into account domain flexibility. Refinement of the structures was done using the CCP4 suite[3,6,19] and COOT.[20] Full data collection and refinement statistics are reported in Table 1.

Table 1. Data Collection and Refinement Statistics for the Three MELK−Ligand Complexes

	MELK+ AMP−PNP	MELK+ Cpd1	MELK+ Cpd2
PDB ID	4BL1	4BKZ	4BKY
space group	$P2_12_12_1$	$P2_12_12_1$	$P2_12_12_1$
cell parameters (Å)			
a	60.02	60.44	59.88
b	63.81	63.15	64.13
c	92.05	95.31	92.58
resolution (Å)	2.60	2.20	1.83
R_{merge} (%)[a]	0.13 (0.72)	0.070 (0.48)	0.077 (0.72)
completeness (%)[a]	99.9 (99.7)	98.7 (99.5)	99.4 (100.0)
unique reflections	11375	18810	31888
redundancy[a]	5.5 (4.9)	4.5 (4.6)	4.9 (5.0)
I/σ[a]	8.9 (2.0)	11.6 (3.2)	11.2 (2.1)
R (%)	18.4	20.1	20.4
R_{free} (%)	26.0	24.0	22.3
rms bond length (Å)	0.02	0.010	0.007
rms angles (°)	2.67	1.577	1.487

[a]Values in parentheses are for reflections in the highest resolution shell.

RESULTS

HTS Campaign and Hit Identification. An HTS campaign was performed of our proprietary compound collection, using the KinaseGlo assay. The HTS campaign resulted in identification of roughly 100 hits with IC_{50} values of less than 0.1 μM that belong to several different chemical classes. Two such HTS hits, Cpd1 and Cpd2 (Chart 1), were selected for structural studies based on their potency, selectivity, and chemical diversity. They were then tested on a panel of 50 kinases (complete list in Table S1, Supporting Information) to explore their selectivity. Cpd1 belongs to the benzodipyrazole class[21] and displays an IC_{50} of 0.027 μM on MELK, with activities below 1 μM on only three other kinases (Haspin, GSK3β, and CDK2/CyclinA, Figure S6, Supporting Information). Cpd2 is from the pyrrolopyrazole class,[22] with an IC_{50} of 0.012 μM on MELK and displaying inhibition of seven further kinases with a potency below 1 μM (AKT1, FLT3, PKCβ, PDK1, RET, PAK4, and PKAα; Figure S6, Supporting Information).

Protein Production and Crystallization. Efforts aimed at obtaining MELK protein crystals were focused on two constructs, one containing the isolated kinase domain (aa 2−266) and the other containing the kinase and UBA domains (aa 2−340). In our hands, the isolated kinase domain gave low yields and was deemed unsuitable for structural studies. In contrast, the construct consisting of the kinase and UBA domains was expressed with good yields as a highly pure, stable, monomeric enzyme. The protein used for structural studies was dephosphorylated, and LC-MS analysis confirmed the complete absence of phosphorylation. The dephosphorylation step proved to be fundamental for obtaining diffraction-quality crystals, which could then be easily reproduced by seeding.

Overall Structure of MELK Catalytic and UBA Domains. Structural analysis revealed that the kinase domain adopts the characteristic bilobal kinase fold typical of all tyrosine and Ser/Thr kinases. The smaller N-terminal lobe is composed of a five-stranded antiparallel β-sheet and a single α-helix (αC). The larger C-terminal lobe is mainly α-helical and contains the regulatory activation loop. The cavity between the N- and C-terminal lobes and the hinge region that interconnects the two defines the binding site for ATP and ATP competitive inhibitors (Figure 1A). A 20 amino acid long, unstructured linker connects the C-terminus of the catalytic domain to the UBA domain (aa 284−327). The UBA domain adopts a compact conformation consisting of three α-helices organized in a "U"-shaped fold, with helix α1 antiparallel to α3.

MELK in Complex with AMP-PNP. The 2.6 Å MELK structure in complex with the ATP analogue, AMP-PNP (Table 1) reveals that apart from the disordered activation loop, MELK displays the characteristics of an active kinase. These include proper positioning of the αC helix as indicated by the salt bridge between the catalytic residues Lys40 and Glu57 and the fact that the N-terminal portion of the activation loop adopts a typically active (DFG-in) conformation. Residues 156−170 of the activation loop are not visible in the electron density, likely due to the flexibility of this region which is quite common in unphosphorylated kinases. However, the N-terminal activation loop fragment that could be modeled

Chart 1. Chemical Structures of Cpd1 and Cpd2

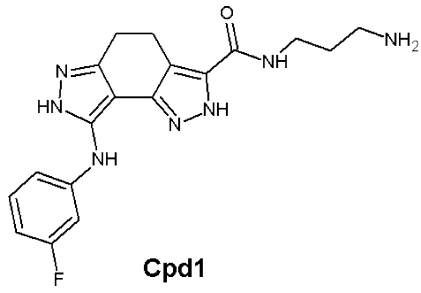

Cpd1

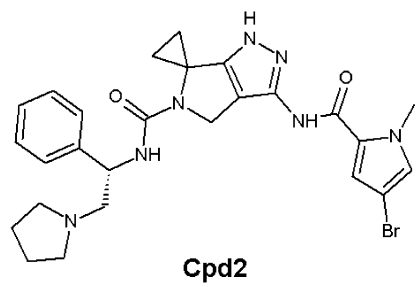

Cpd2

dx.doi.org/10.1021/bi4005864 | Biochemistry 2013, 52, 6380−6387

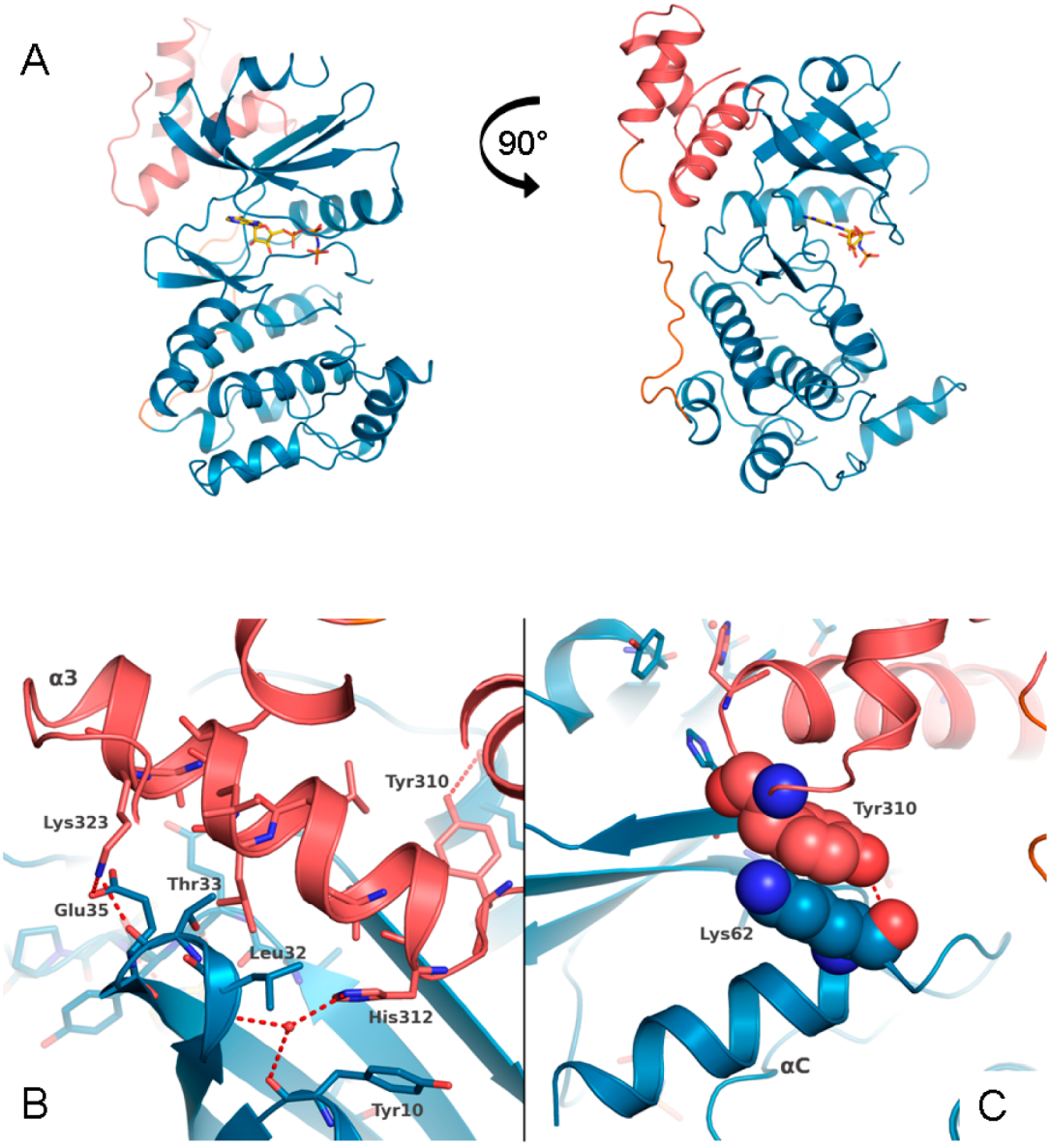

Figure 1. (A) Ribbon representation of the structure of MELK (kinase domain: blue ribbons, UBA domain: red ribbons, linker: orange ribbons) in complex with AMP-PNP (PDB ID 4BL1), showing the relative arrangement of the two domains and the linker connecting them. AMP-PNP, bound to the kinase active site, is shown in stick representation. (B) Hydrogen bond network of helix a3 (red ribbons) with the kinase N-lobe (blue ribbons). (C) Stacking interaction between Tyr310 from helix a3 (red spheres) and Lys62 from helix αC (blue spheres).

(from the DFG Asp150 to Ala155) is clearly in a DFG-in conformation. The AMP-PNP ligand displays the expected nucleotide binding mode (Figure S7, Supporting Information), with the adenine ring binding to the hinge region via two hydrogen bonds with the backbone carbonyl of Glu87 and the amino group of Cys89, respectively. The ribose moiety establishes polar interactions with Glu93, while conserved residues Lys40 and Asp150 hold the imidodiphosphate moiety in place.

MELK UBA Domain. The interaction between the MELK UBA and kinase domains is similar to that observed for the previously described MARK structures.[23] More specifically, in MELK the UBA domain binds to the N-lobe mainly through helix α3, which forms numerous hydrophobic contacts between its Leu-rich core and the N-lobe β-sheet (strands β3 and β4) of the kinase domain. The two polar ends of helix α3 are able to establish a network of hydrogen bonds with N-lobe residues. His312 binds through a conserved water molecule to the amino group of Leu32 and to the carbonyl of Tyr10, while the terminal amine group of Lys323 interacts with the backbone carbonyl of Thr33 and with the carboxylate of Glu35 (Figure 1B,C). Moreover, the side chain of Tyr310 on the loop between α2–α3 is stacked against the hydrophobic patch formed by the side chain of Lys62 on helix αC and the hydrophobic residue Leu72 (strand β4), contributing to keeping helix αC in its active "in" conformation.

MELK in Complex with Cpd1. The 2.20 Å structure of MELK in complex with Cpd1 reveals that its benzodipyrazole core occupies the adenine-binding region and that the pyrazole nitrogen atoms make the canonical donor–acceptor hydrogen bonds with the backbone of residues Glu87 and Cys89. Hydrophobic interactions that contribute to binding include the MELK residues Ile17, Val25, Ala38, Cys70, Leu86 (the "gatekeeper" residue), Leu139, and Ile149 (DFG-1, Figure 2A).

dx.doi.org/10.1021/bi4005864 | *Biochemistry* 2013, 52, 6380–6387

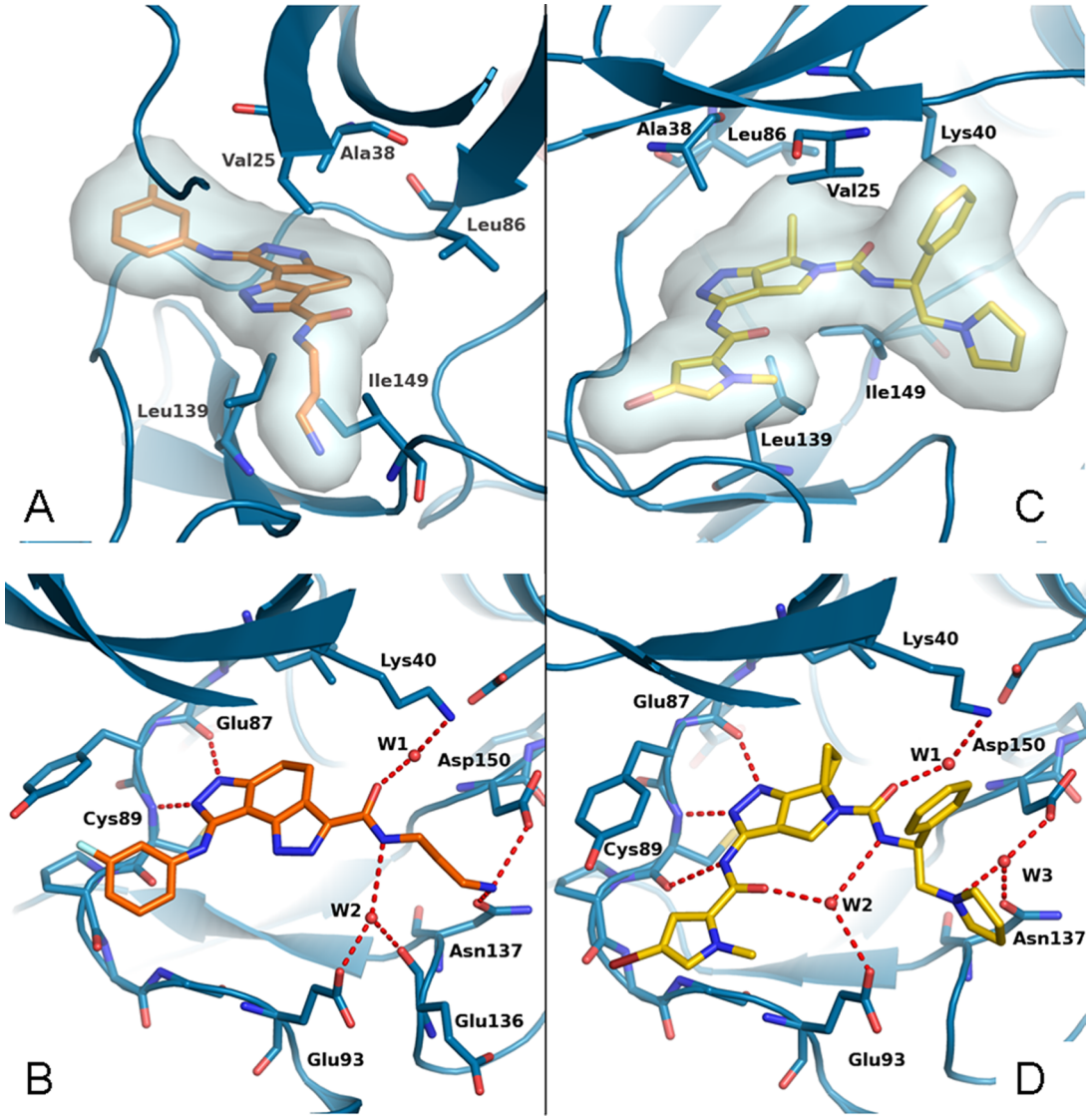

Figure 2. Representation of the hydrophobic (A) and polar (B) interactions between Cpd1 (orange carbon atoms) and the MELK active site (blue ribbons, blue carbon atoms). Representation of the hydrophobic (C) and polar (D) interactions between Cpd2 (yellow carbon atoms) and the MELK active site (blue ribbons, blue carbon atoms).

The inhibitor extends toward helix αC occupying the phosphate region, where the amide carbonyl interacts with the conserved Lys40 via a water molecule (W1). The amide nitrogen makes a water-mediated interaction (W2) with the carboxylate of Glu93, (helix αD) and the carbonyl of Glu136. The aminopropylic chain interacts via hydrogen bonds with the carboxylate of Asp150 (DFG) and the carboxamide of Asn137 (catalytic loop, Figure 2B). The presence of a meta-fluorophenyl moiety facing the hinge region induces Tyr88 to adopt a different conformation, rotating toward the solvent. This conformational change suggests that the presence of a small substituent in the meta position of the phenyl ring, though tolerated, is not favorable for a kinase with a bulky residue in the gatekeeper+2 position. We can speculate that larger substituents would be detrimental to compound potency (see Figure S8, Supporting Information).

MELK in Complex with Cpd2. The 1.83 Å structure of MELK in complex with Cpd2 reveals that its pyrrolopyrazole core is stacked between by Val25, Leu139, Ile149 (DFG-1 residue); its cyclopropyl points toward the gatekeeper Leu86 and makes favorable contacts with Ala38. Moreover, the phenyl ring of the amide substituent is stacked against the alkylic portion of Lys40 (Figure 2C). The aminopyrazole moiety is anchored to the hinge via a donor−acceptor−donor pattern of hydrogen bonds with Glu87 and Cys89. Interestingly, Cpd2 also establishes a rich network of water-mediated polar interactions with MELK; three water molecules bridge between the inhibitor and key active site residues. A conserved water molecule (W1) bridges between Lys40 and the amide oxygen located between the pyrrolopyrazole core and the phenyl-(pyrrolidinethyl) group, while another water molecule (W2) mediates the interaction between the carboxylate of Glu93 and the two amide groups of Cpd2. Furthermore, a third water molecule (W3) bridges between the pyrrolidine moiety of Cpd2, the carboxylate of Asp150 (DFG), and the carboxamide of Asn137 (Figure 2D). The aromatic substituent points toward the hydrophobic interior of the glycine-rich loop, stabilizing it in a semi-open conformation.

Activity of Cpd2 in Cells. Cpd2 was evaluated for its effects on cell growth in cell lines originating from various

dx.doi.org/10.1021/bi4005864 | *Biochemistry* 2013, 52, 6380−6387

human tumor types including A2780 (ovarian carcinoma), LNCaP (prostate carcinoma), and MDA-MB-468 (breast carcinoma) cells. Incubation of cells for 72 h with the compound at different concentrations revealed antiproliferative activity with an IC_{50} of 0.25, 0.36, and 2.2 μM respectively, as reported in Figure 3A.

A)

A2780 (IC_{50}) ovarian cancer	LNCaP (IC_{50}) prostate cancer	MDA-MB-468 (IC_{50}) breast cancer
0.25 μM	0.36 μM	2.2 μM

B)

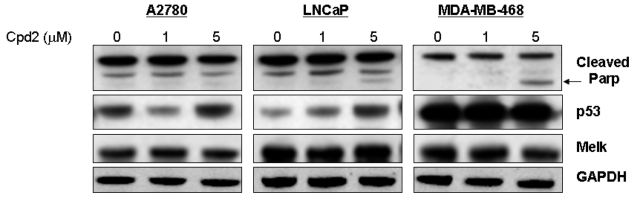

Figure 3. Activity of Cpd2 in cells. (A) In vitro cell proliferation after treatment of three tumor cell lines with the compound at different doses for 72 h. (B) Analysis of cell lysates treated with the indicated doses of the compound for 24 h and immunoblotted with the reported antibodies.

Furthermore, to confirm the pharmacological mechanism of action in cells, we determined the ability of Cpd2 to increase p53 in LNCaP and A2780, both p53 wild type cell lines. As shown in Figure 3B, treatment with 1 μM and 5 μM of compound for 24 h resulted in increased p53 protein levels in both cell lines, as observed by Gu et al.[24] following MELK gene silencing. In the MDA-MB-468 breast cell line which possesses mutant p53, we instead observed increased PARP cleavage, indicative of caspase-dependent apoptosis, following compound treatment. Differently from what has been reported for siomycin A,[25] Cpd2 did not reduce MELK protein levels.

DISCUSSION

The UBA domain is a unique conserved feature of the AMPK-related kinase family. While being the only kinase family containing this kind of domain, UBA domains from AMPK-related kinases display a characteristic "U-shaped" fold, differing significantly from the canonical "N-shaped" UBA fold found in other protein families, in the orientation of helix α3 (Figure S9, Supporting Information).[26]

The presence or absence of the MELK UBA domain has been shown to affect MELK activity,[12] suggesting a regulatory role. The structural data reported here provide fresh evidence to support this hypothesis. The interactions established between Tyr310 (UBA domain), Lys62, and Leu72 (N-lobe) appear in fact to play a key role in stabilizing the αC helix in its active conformation. Furthermore, a similar arrangement between aromatic residues belonging to regulatory domains and the C-terminal amino acid in helix αC has been observed for a variety of protein kinases both in active and inactive conformations. An appropriate such example is the Ser/Thr kinase Akt1, where Tyr474 of the hydrophobic motif is engaged in a similar kind of interaction, with the same geometry, with Gln203 in helix αC (e.g., PDB 3CQW, Figure S10, Supporting Information). We therefore suggest that the UBA domain could have an analogous regulatory role, acting as a switch between different kinase conformations.

The two HTS hits whose structural data are presented here display the classical type I, DFG-in binding mode of ATP-competitive kinase inhibitors. Both compounds occupy the whole MELK active site and are involved in a rich network of both hydrophobic and polar contacts, either direct or water-mediated. It is worth noting that, besides the canonical interactions with the hinge region, both Cpd2 and Cpd1 are engaged in polar contacts with Asp150 (DFG), Glu93 (belonging to helix αD), and Asn137 (on the catalytic loop). These interactions appear to be of significant importance for binding and could be exploited for the design of compounds with improved potency.

Comparison of the two structures also suggests that Cpd2 displays a superior "shape complementarity" (Figure S11, Supporting Information) with the MELK active site as compared to Cpd1. Superposition of the benzodipyrazole onto the pyrrolopyrazole core shows that the latter fits better into the binding site, plunging ~1 Å deeper into the pocket. Moreover, the MELK-Cpd2 complex has a larger interface area than MELK-Cpd1 (511.5 $Å^2$ and 392.6 $Å^2$, respectively). We can hypothesize that Cpd1 does not optimally fill the cavity due to the steric hindrance of the meta-fluorophenyl substituent clashing with Tyr88. Furthermore, Cpd2 has an aromatic moiety that stabilizes the glycine-rich loop in a semi-open conformation, whereas the structure of MELK in complex with Cpd1 displays a partially disordered Glycine-rich loop. Taken together, these data indicate that Cpd2 might be a more promising compound than Cpd1 for further studies.

We therefore analyzed the effect of Cpd2 on three cancer cell lines in which MELK is reported to be highly expressed: A2780 (ovarian cancer), MDA-MB-468 (ER-negative breast cancer), and LNCaP (prostate cancer).[2,5,7] These studies revealed promising activity in terms of inhibition of cell proliferation and also yielded preliminary evidence of in-mechanism biological activity, with induction of increased p53 levels, at least in A2780 and LNCaP cell lines, consistent, for Cpd2, with a molecular mechanism acting through MELK inhibition.

Moreover, further studies in the context of biomarker identification are warranted to elucidate the exact mechanism of MELK. Overexpression of MELK at the RNA and protein level was reported for multiple human tumor samples and cell lines. MELK has been implicated in cancer stem-cell formation/maintenance,[2] and it plays a key role in mammary carcinogenesis through inhibition of the pro-apoptotic function of Bcl-GL.[4] In addition, it has been found to be upregulated in glioblastoma as well as in triple negative breast cancer and high-grade prostate.[7,8,27] These findings suggest a critical role of MELK in the proliferation of brain tumors, including their stem cells as well as of breast and prostate carcinoma tumors and indicate that it may be a compelling molecular target for treatment of this type of tumors.

In conclusion, our data provide insights into the structure and inhibition of MELK. Our findings shed some light on the arrangement, conformation, and putative regulatory role of the UBA domain. Moreover, we characterized its active site by studying the binding mode of two diverse nanomolar inhibitors. This allowed us to identify and evaluate the active site hot spots, thus laying the basis for structure-based drug design efforts aimed at improving compound potency and selectivity.

dx.doi.org/10.1021/bi4005864 | *Biochemistry* 2013, 52, 6380−6387

■ ASSOCIATED CONTENT

Supporting Information

Supplementary tables and figures. This material is available free of charge via the Internet at http://pubs.acs.org.

Accession Codes

Atomic coordinates have been deposited in the Protein Data Bank as entries 4BL1, 4BKZ, and 4BKY.

■ AUTHOR INFORMATION

Corresponding Author

*E-mail: giulia.canevari@nervianoms.com; phone: 0039 0331581113.

Present Address

†Vertex Pharmaceuticals (Europe) Limited, 88 Milton Park, Abingdon, Oxfordshire OX14 4RY, UK.

Notes

The authors declare no competing financial interest.

■ ACKNOWLEDGMENTS

We thank Mauro Paolucci, Nilla Avanzi, the Assay Development, the Biochemical Screening group, and the HIDE group for performing the HTS campaign; Pamela Rosettani, Elisa Dioguardi, and Silvia Salis for initial crystallization activities; the Cell Proliferation Group for cellular assays.

■ ABBREVIATIONS

MELK, maternal embryonic leucine zipper kinase; AMP-PNP, adenosine 5′-(β,γ-imido)triphosphate; HTS, high throughput screening

■ REFERENCES

(1) Gil, M., Yang, Y., Lee, Y., Choi, I., and Ha, H. (1997) Cloning and expression of a cDNA encoding a novel protein serine/threonine kinase predominantly expressed in hematopoietic cells. *Gene 195*, 295−301.

(2) Gray, D., Jubb, A. M., Hogue, D., Dowd, P., Kljavin, N., Yi, S., Bai, W., Frantz, G., Zhang, Z., Koeppen, H., de Sauvage, F. J., and Davis, D. P. (2005) Maternal embryonic leucine zipper kinase/murine protein serine-threonine kinase 38 is a promising therapeutic target for multiple cancers. *Cancer Res. 65*, 9751−9761.

(3) Rhodes, D. R., Yu, J., Shanker, K., Deshpande, N., Varambally, R., Ghosh, D., Barrette, T., Pandey, A., and Chinnaiyan, A. M. (2004) Large-scale meta-analysis of cancer microarray data identifies common transcriptional profiles of neoplastic transformation and progression. *Proc. Natl. Acad. Sci. U. S. A. 101*, 9309−9314.

(4) Lin, M. L., Park, J. H., Nishidate, T., Nakamura, Y., and Katagiri, T. (2007) Involvement of maternal embryonic leucine zipper kinase (MELK) in mammary carcinogenesis through interaction with Bcl-G, a pro-apoptotic member of the Bcl-2 family. *Breast Cancer Res. 9*, R17.

(5) Speers, C., Tsimelzon, A., Sexton, K., Herrick, A. M., Gutierrez, C., Culhane, A., Quackenbush, J., Hilsenbeck, S., Chang, J., and Brown, P. (2009) Identification of novel kinase targets for the treatment of estrogen receptor-negative breast cancer. *Clin. Cancer Res. 15*, 6327−6340.

(6) Nakano, I., Paucar, A. A., Bajpai, R., Dougherty, J. D., Zewail, A., Kelly, T. K., Kim, K. J., Ou, J., Groszer, M., Imura, T., Freije, W. A., Nelson, S. F., Sofroniew, M. V., Wu, H., Liu, X., Terskikh, A. V., Geschwind, D. H., and Kornblum, H. I. (2005) Maternal embryonic leucine zipper kinase (MELK) regulates multipotent neural progenitor proliferation. *J. Cell Biol. 170*, 413−427.

(7) Kuner, R., Falth, M., Pressinotti, N. C., Brase, J. C., Puig, S. B., Metzger, J., Gade, S., Schafer, G., Bartsch, G., Steiner, E., Klocker, H., and Sultmann, H. (2013) The maternal embryonic leucine zipper kinase (MELK) is upregulated in high-grade prostate cancer. *J. Mol. Med. (Berlin) 91*, 237−248.

(8) Nakano, I., Masterman-Smith, M., Saigusa, K., Paucar, A. A., Horvath, S., Shoemaker, L., Watanabe, M., Negro, A., Bajpai, R., Howes, A., Lelievre, V., Waschek, J. A., Lazareff, J. A., Freije, W. A., Liau, L. M., Gilbertson, R. J., Cloughesy, T. F., Geschwind, D. H., Nelson, S. F., Mischel, P. S., Terskikh, A. V., and Kornblum, H. I. (2008) Maternal embryonic leucine zipper kinase is a key regulator of the proliferation of malignant brain tumors, including brain tumor stem cells. *J. Neurosci. Res. 86*, 48−60.

(9) Pickard, M. R., Green, A. R., Ellis, I. O., Caldas, C., Hedge, V. L., Mourtada-Maarabouni, M., and Williams, G. T. (2009) Dysregulated expression of Fau and MELK is associated with poor prognosis in breast cancer. *Breast Cancer Res. 11*, R60.

(10) Chung, S., Suzuki, H., Miyamoto, T., Takamatsu, N., Tatsuguchi, A., Ueda, K., Kijima, K., Nakamura, Y., and Matsuo, Y. (2012) Development of an orally-administrative MELK-targeting inhibitor that suppresses the growth of various types of human cancer. *Oncotarget 3*, 1629−1640.

(11) Manning, G., Whyte, D. B., Martinez, R., Hunter, T., and Sudarsanam, S. (2002) The protein kinase complement of the human genome. *Science 298*, 1912−1934.

(12) Beullens, M., Vancauwenbergh, S., Morrice, N., Derua, R., Ceulemans, H., Waelkens, E., and Bollen, M. (2005) Substrate specificity and activity regulation of protein kinase MELK. *J. Biol. Chem. 280*, 40003−40011.

(13) Felder, E. R., Badari, A., Disingrini, T., Mantegani, S., Orrenius, C., Avanzi, N., Isacchi, A., and Salom, B. (2012) The generation of purinome-targeted libraries as a means to diversify ATP-mimetic chemical classes for lead finding. *Mol. Diversity 16*, 27−51.

(14) Pevarello, P., Brasca, M. G., Amici, R., Orsini, P., Traquandi, G., Corti, L., Piutti, C., Sansonna, P., Villa, M., Pierce, B. S., Pulici, M., Giordano, P., Martina, K., Fritzen, E. L., Nugent, R. A., Casale, E., Cameron, A., Ciomei, M., Roletto, F., Isacchi, A., Fogliatto, G., Pesenti, E., Pastori, W., Marsiglio, A., Leach, K. L., Clare, P. M., Fiorentini, F., Varasi, M., Vulpetti, A., and Warpehoski, M. A. (2004) 3-Amino-pyrazole inhibitors of CDK2/cyclin A as antitumor agents. 1. Lead finding. *J. Med. Chem. 47*, 3367−3380.

(15) Leslie, A. G. W., and a. P., H. R. (2007) Processing diffraction data with Mosflm. *Evolving Methods Macromol. Crystallogr. 245*, 41−51.

(16) Leslie, A. G. W. (1992) Recent changes to the MOSFLM package for processing film and image plate data. *Protein Crystallogr.*, 26.

(17) Evans, P. R. E. (1997) Scala. *Protein Crystallogr. 33*, 22−24.

(18) McCoy, A. J., Grosse-Kunstleve, R. W., Adams, P. D., Winn, M. D., Storoni, L. C., and Read, R. J. (2007) Phaser crystallographic software. *J. Appl. Crystallogr. 40*, 658−674.

(19) Winn, M. D., Ballard, C. C., Cowtan, K. D., Dodson, E. J., Emsley, P., Evans, P. R., Keegan, R. M., Krissinel, E. B., Leslie, A. G., McCoy, A., McNicholas, S. J., Murshudov, G. N., Pannu, N. S., Potterton, E. A., Powell, H. R., Read, R. J., Vagin, A., and Wilson, K. S. (2011) Overview of the CCP4 suite and current developments. *Acta Crystallogr., Sect. D: Biol. Crystallogr. 67*, 235−242.

(20) Emsley, P., Lohkamp, B., Scott, W. G., and Cowtan, K. (2010) Features and development of Coot. *Acta Crystallogr., Sect. D: Biol. Crystallogr. 66*, 486−501.

(21) D'Alessio, R., Bargiotti, A., Metz, S., Brasca, M. G., Cameron, A., Ermoli, A., Marsiglio, A., Polucci, P., Roletto, F., Tibolla, M., Vazquez, M. L., Vulpetti, A., and Pevarello, P. (2005) Benzodipyrazoles: a new class of potent CDK2 inhibitors. *Bioorg. Med. Chem. Lett. 15*, 1315−1319.

(22) Fancelli, D., Berta, D., Bindi, S., Cameron, A., Cappella, P., Carpinelli, P., Catana, C., Forte, B., Giordano, P., Giorgini, M. L., Mantegani, S., Marsiglio, A., Meroni, M., Moll, J., Pittala, V., Roletto, F., Severino, D., Soncini, C., Storici, P., Tonani, R., Varasi, M., Vulpetti, A., and Vianello, P. (2005) Potent and selective Aurora inhibitors identified by the expansion of a novel scaffold for protein kinase inhibition. *J. Med. Chem. 48*, 3080−3084.

(23) Marx, A., Nugoor, C., Panneerselvam, S., and Mandelkow, E. (2010) Structure and function of polarity-inducing kinase family

MARK/Par-1 within the branch of AMPK/Snf1-related kinases. *FASEB J. 24*, 1637−1648.
(24) Gu, C., Banasavadi-Siddegowda, Y. K., Joshi, K., Nakamura, Y., Kurt, H., Gupta, S., and Nakano, I. (2013) Tumor-specific activation of the C-JUN/MELK pathway regulates glioma stem cell growth in a p53-dependent manner. *Stem Cells 31*, 870−881.
(25) Nakano, I., Joshi, K., Visnyei, K., Hu, B., Watanabe, M., Lam, D., Wexler, E., Saigusa, K., Nakamura, Y., Laks, D. R., Mischel, P. S., Viapiano, M., and Kornblum, H. I. (2011) Siomycin A targets brain tumor stem cells partially through a MELK-mediated pathway. *Neurol. Oncol. 13*, 622−634.
(26) Jaleel, M., Villa, F., Deak, M., Toth, R., Prescott, A. R., Van Aalten, D. M., and Alessi, D. R. (2006) The ubiquitin-associated domain of AMPK-related kinases regulates conformation and LKB1-mediated phosphorylation and activation. *Biochem. J. 394*, 545−555.
(27) Komatsu, M., Yoshimaru, T., Matsuo, T., Kiyotani, K., Miyoshi, Y., Tanahashi, T., Rokutan, K., Yamaguchi, R., Saito, A., Imoto, S., Miyano, S., Nakamura, Y., Sasa, M., Shimada, M., and Katagiri, T. (2013) Molecular features of triple negative breast cancer cells by genome-wide gene expression profiling analysis. *Int. J. Oncol. 42*, 478−506.